Author Manuscript

Author Manuscript

Author Manuscript

Author Manuscript

HHS Public Access

Author manuscript

J Am Chem Soc. Author manuscript; available in PMC 2017 February 01.

Published in final edited form as:

J Am Chem Soc. 2015 August 05; 137(30): 9704–9715. doi:10.1021/jacs.5b05229.

Activation of Dioxygen by a TAML Activator in Reverse Micelles: Characterization of an $Fe^{III}Fe^{IV}$ Dimer and Associated Catalytic Chemistry

Liang L. Tang, **William A. Gunderson**, **Andrew C. Weitz**, **Michael P. Hendrich***, **Alexander D. Ryabov***, and **Terrence J. Collins***

Department of Chemistry, Carnegie Mellon University, 4400 Fifth Avenue, Pittsburgh, Pennsylvania 15213, United States

Abstract

Iron TAML activators of peroxides are functional catalase-peroxidase mimics. Switching from hydrogen peroxide (H_2O_2) to dioxygen (O_2) as the primary oxidant was achieved by using a system of reverse micelles of Aerosol OT (AOT) in *n*-octane. Hydrophilic TAML activators are localized in the aqueous microreactors of reverse micelles where water is present in much lower abundance than in bulk water. *n*-Octane serves as a proximate reservoir supplying O_2 to result in partial oxidation of Fe^{III} to Fe^{IV}-containing species, mostly the $Fe^{III}Fe^{IV}$ (major) and $Fe^{IV}Fe^{IV}$ (minor) dimers which coexist with the Fe^{III} TAML monomeric species. The speciation depends on the pH and the degree of hydration w_0, viz., the amount of water in the reverse micelles. The previously unknown $Fe^{III}Fe^{IV}$ dimer has been characterized by UV–vis, EPR, and Mössbauer spectroscopies. Reactive electron donors such as NADH, pinacyanol chloride, and hydroquinone undergo the TAML-catalyzed oxidation by O_2. The oxidation of NADH, studied in most detail, is much faster at the lowest degree of hydration w_0 (in "drier micelles") and is accelerated by light through NADH photochemistry. Dyes that are more resistant to oxidation than pinacyanol chloride (Orange II, Safranine O) are not oxidized in the reverse micellar media. Despite the limitation of low reactivity, the new systems highlight an encouraging step in replacing TAML peroxidase-like chemistry with more attractive dioxygen-activation chemistry.

Graphical abstract

***Corresponding Authors:** hendrich@andrew.cmu.edu; ryabov@andrew.cmu.edu; tc1u@andrew.cmu.edu.

Supporting Information

Experimental details, HPLC methods, and additional results (Tables S1–S3). UV–vis data for **1a** under different conditions (Figures S1, S4, S10). UV–vis analysis of substrate degradations under varied conditions in reverse micelles (Table S4, Figures S7–S9, and Figures S11–S13). EPR experimental results and simulations (Figures S2, S3, and S5). Raw Mössbauer spectra (Figure S6).The Supporting Information is available free of charge on the ACS Publications website at DOI: 10.1021/jacs.5b05229.

Notes

The authors declare no competing financial interest.

Author Manuscript Author Manuscript Author Manuscript Author Manuscript

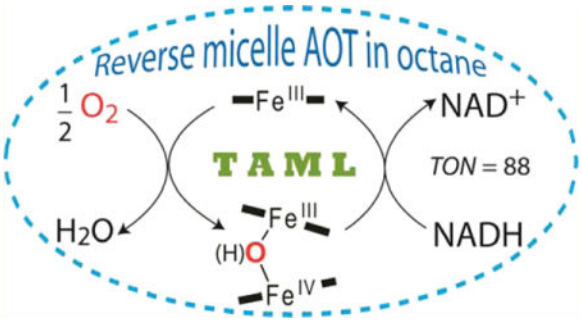

INTRODUCTION

TAML activators of peroxides (**1**, Chart 1) are a family of green oxidation catalysts that function similarly to catalase-peroxidase enzymes.[1–3] In the resting state, Fe^{III} occupies the cavity of the deprotonated tetraamido macrocyclic ligand and directs the oxidative power of hydrogen peroxide (H_2O_2) at different targets in aqueous solution. TAML activators are similar to peroxidases mechanistically in that Fe^{IV}4 and Fe^{V}5 relatives of enzymatic compounds II and I, respectively,[6] have been detected and characterized. Superior activity of TAML activators has been demonstrated for H_2O_2 or organic peroxides catalysis in water.[7–11] While H_2O_2 is a desirable green oxidant, its concentrated solutions are potentially hazardous[12] and it comes at a real production and delivery cost. In contrast, dioxygen (O_2) is freely available and is the principal biochemical oxidizing agent. Therefore, our foremost strategic goal for TAML activator-based catalysis has been to master the use of O_2 as the primary oxidant.[13–15] TAML activators in the ferric state are readily oxidized by O_2 in *weakly* coordinating organic solvents such as CH_2Cl_2 to produce Fe^{IV} species.[16] While iron(IV) TAML activators have been shown to oxidize some substrates in organic solvents, comparably efficient catalysis to the aqueous systems has yet to be observed.[2,16,17] TAML catalysis in water is characteristically conducted aerobically. Yet unless an oxidant such as hydrogen peroxide is added, no catalysis is observed, with the current suite of catalysts, bulk water appears thus far to be inimical to facile oxygen activation. Two conditions appear to be favorable for dioxygen activation. First, the TAML medium should be rich in O_2: under ambient conditions, this situation is best accommodated in organic solvents. Second, water should surround TAML activators for maintaining high catalytic activity. Recent studies have shown that some, but not too much, water is important for oxidations of ferric TAMLs by organic peroxides in organic solvents.[18–22] The amount of water should not be large because H_2O molecules compete with O_2 for coordination sites on Fe^{III}. Hydrogen bonding and/ or polarity effects may also play some role. In bulk water, iron(III) TAML activators are six-coordinate species with two axial water ligands,[23] which is consistent with the observed inactivity of oxygen activation where 55 M H_2O effectively blocks O_2 binding to Fe^{III}.

The two above conditions are in principle attainable using reverse micelles.[24–26] Micellar media are nowadays common for catalytic applications.[27] A system of reverse micelles is composed of aqueous microparticles in organic media such as *n*-octane (Figure 1). At the level of the individual microreactors, the micellar wall is composed of surfactant molecules; the sodium salt of bis(2-ethylhexyl) sulfosuccinate (Aerosol OT or AOT) is commonly

Author Manuscript Author Manuscript Author Manuscript Author Manuscript

used.[28] The hydrophobic tails are directed at the bulk organic medium, whereas the hydrophilic heads comprise the encapsulating surface of the microreactor inner water cavity.[26] Chemical and enzymatic catalysis in reverse micellar systems is well documented.[24,25] TAML activators have excellent solubility properties for guaranteeing sequestration in reverse micellar microreactors; the *n*-octanol/water partition coefficient for **1a** (Chart 1) is 0.036.[29,30] The size of the microreactor and the water content within is determined by the degree of hydration, i.e., the water-to-surfactant molar ratio in the bulk system: $w_0 = [H_2O]/[AOT]$.[26] The solubility of O_2 in *n*-octane is 1 order of magnitude higher than in water,[31] and therefore TAML-containing reverse micelles will be surrounded by an O_2-rich medium favorable for the oxidation of Fe^{III}. At the same time, Fe^{III} will be in contact with water, the amount of which is regulated by the degree of hydration w_0.

In this work we show that oxidative catalysis is possible for reactive electron donors using **1** in reverse micelles of AOT in *n*-octane *in the absence* of an added oxidant such as H_2O_2 but in the presence of ambient O_2. Reverse micelles of AOT have been thoroughly investigated[28] and, importantly, have often been used as media for catalysis by peroxidase enzymes,[26,32] the biocatalysts closest to TAMLs.[8] Here we demonstrate the following. (i) Dioxygen oxidizes **1a** in the reverse micellar medium to multiple iron(IV)-containing species. (ii) These species coexist with the starting iron(III) TAML. (iii) The iron(IV) species are the earlier reported homovalent dimer $Fe^{IV}Fe^{IV}$ **2a** and the less-oxidized, previously unknown heterovalent dimer $Fe^{III}Fe^{IV}$ **3a**. (iv) Compound **3a** in reverse micellar medium has been detected by EPR and characterized by UV–vis, EPR, and Mössbauer spectroscopies in glycerol-containing aqueous solutions at −20 °C. (v) TAML activators in this reverse micellar medium catalyze the oxidation by O_2 of reactive electron donors such as the dye pinacyanol chloride, NADH, and hydroquinone (Chart 1). (vi) The oxidation of NADH is a photocatalytic process, the rate of which is directly proportional to the flash frequency. (vii) The catalytic activity of TAML activators is a function of both the degree of hydration w_0 and the pH. (viii) The dyes Orange II and Safranin O, which are more resistant to oxidation than PNC, are not oxidized by O_2 in this system.

EXPERIMENTAL SECTION

Materials

All reagents, components of buffer solutions, and solvents were at least ACS reagent grade (Aldrich, Fisher, Acros, Fluka) and were used as received. TAML activators **1a**,**b** were obtained from GreenOx Catalysts, Inc.[57]Fe enriched **1a** was synthesized as previously reported.[33,34] *n*-Octane (99%+, Acros) was used as received. Stock solutions of **1a** (0.0010 and 0.027 M) and **1b** (0.0010 M) were prepared in the 0.01 M buffered aqueous solutions using phosphate for pH 8 and 12 but carbonate for pH 10; all were stored in a fridge at 4 °C. Hydroquinone (1.0 mg, Acros, 99.5%) recrystallized from acetone was dissolved in a mixture of 0.1 M AOT in *n*-octane (15.3 mL) and 48 μL of 0.01 M phosphate (pH 8 or 12) or carbonate (pH 10) buffer. This allowed the preparation of the 6.0×10^{-4} M solution of HQ in reverse micelles with lower w_0. The solutions with larger w_0 were made by adding aqueous buffer to the stock solution. Stock solutions of H_2O_2 were prepared from 30% H_2O_2, and the concentration was determined by measuring the absorption at 230 nm (ε =

Author Manuscript Author Manuscript Author Manuscript Author Manuscript

72.4 M^{-1} cm^{-1}).[35] AOT (Aerosol OT, BioXtra 99%+, Aldrich) was either used as received or additionally purified by activated charcoal and dried in a vacuum oven for 40 h as recommended elsewhere.[36] Solutions of AOT in *n*-octane (0.1 M) were shown to be peroxide-free using the peroxide test strips (0.5–25 ppm, EM Quant).[37] The AOT solutions were also treated with aqueous KI[37] and no color change due to the formation of I_3^- was observed. Negative peroxide tests were obtained for AOT before and after the purification. Reverse micelles of various w_0 were prepared by adding a corresponding amount of the aqueous buffer of known pH to 0.1 M AOT in *n*-octane. For example, the sample with w_0 7 and pH 8 was prepared by adding the buffer (25 μL, pH 8) to 1975 μL of 0.1 M AOT followed by vigorous shaking. Concentrations of all components reported throughout refer to the entire volume of the solution including *n*-octane, AOT, and buffer components.

NADH and NAD^+ were purchased from Sigma-Aldrich and used as received. Their stock solutions were prepared daily using HPLC grade water. The extinction coefficients (ε) of NADH in reverse micelles were measured after adding 0.1 M AOT in *n*-octane to 2.0 mg NADH dissolved in 60 μL of pure water in a 5 mL volumetric flask. The ε_{340} values of 4760, 4980, 5070, 5130, and 5200 (all ±20) M^{-1} cm^{-1} at w_0 3, 7, 10, 15, and 25, respectively, were used in kinetic measurements. Pinacyanol chloride (Aldrich) was used without further purification. Orange II (Sigma-Aldrich) was recrystallized from 1:3 H_2O:EtOH. Safranin O (Acros) was used as received. Alcohol dehydrogenase from *Saccharomyces cerevisiae* was a Sigma-Aldrich preparation.

Methods

UV–vis measurements were performed at 25 °C in capped quartz cuvettes (1.0 cm) using either a photodiode array Agilent 8453 UV–vis spectrometer equipped with an automatic thermostated eight-cell positioner or a double beam Shimadzu UV 1800 instrument having the thermostated six-cell positioner. HPLC measurements were carried out[38] using a Shimadzu Prominence 2D HPLC instrument equipped with LC-20AB binary pump (method 1) or LC-20AD quaternary pump (method 2), SIL-20A autosampler, and SPD-M20A photodiode array detector (see Supporting Information (SI) for details).

EPR and Mössbauer Measurements

Solutions of **1a** (0.15 mM) in the reverse micelles as prepared above were transferred into EPR tubes and frozen by liquid nitrogen. A solution of H_2O_2 was added to a solution of **1a** (0.5–2.0 mM) in 0.1 M phosphate buffer (pH 11.8), transferred to EPR tubes, and frozen in liquid nitrogen 30 s after the addition of H_2O_2. Samples at low temperature (−20 °C) were prepared in the phosphate buffer containing 50% glycerol (v/v). The temperature was lowered by keeping the solution ~1 cm above a dry ice/acetone bath. Samples for the Mössbauer spectroscopy were prepared by adding 1 equiv of H_2O_2 to a 5 mM solution of ^{57}Fe enriched **1a** at −20 °C as above. When needed, the solutions were split for the Mössbauer cup and EPR studies and frozen simultaneously in liquid nitrogen 30 s after the addition of H_2O_2. X-band (9.66 GHz) EPR spectra were recorded on either a Bruker ESP 300 or a Bruker ELEXSYS-II E500 spectrometer equipped with an Oxford ESR-910 liquid helium cryostat. All experimental data were collected under nonsaturating microwave conditions. The quantification of signals was relative to a CuEDTA spin standard. The

Author Manuscript Author Manuscript Author Manuscript Author Manuscript

microwave frequency and the magnetic field were calibrated with a frequency counter and an NMR gaussmeter, respectively. The temperature was calibrated with resistors (CGR-1-1000) from LakeShore. A modulation frequency of 100 kHz and modulation amplitude of 1 mT was used for all spectra. The analysis of data utilized the standard spin Hamiltonians eqs 1 and 2, where the subscripts 3 and 4 refer to the Fe^{III} and Fe^{IV} iron sites:

$$H = -2J\mathbf{S}_3 \cdot \mathbf{S}_4 + \sum_{i=3,4}[\beta \mathbf{B} \cdot \mathbf{g}_i \cdot \mathbf{S}_i + \mathbf{S}_i \cdot \mathbf{D}_i \cdot \mathbf{S}_i + \mathbf{S}_i \cdot \mathbf{A}_i \cdot \mathbf{I}_i + H_{ni}] \quad (1)$$

$$H_{ni} = -\beta_n g_n \mathbf{B} \cdot \mathbf{I}_i + (eQV_{zzi}/12)[3{I_{zi}}^2 - I_i(I_i+1) + \eta_i({I_{xi}}^2 - {I_{yi}}^2)] \quad (2)$$

Simulations of EPR spectra of **1a** use the relevant parts of eq 1 for a single spin $S = 3/2$, or the electronic parts of eq 1 for **3a**. Mössbauer spectra were recorded using two spectrometers with an available temperature range of 1.5 to 200 K and magnetic fields up to 8.0 T. Isomer shifts are reported relative to Fe metal at 298 K. Data analysis, spin quantification, and simulations of the EPR and Mössbauer spectra were performed with the software SpinCount written by one of the authors (M.P.H.).[39]

RESULTS AND DISCUSSION

A Preliminary Comment on Speciation of Iron in Reverse Micelles

Chart 2 shows species that one might anticipate could coexist in the micellar media. Most of them are known. $Fe^{III}OH_2$ is the starting **1a**. EPR silent diamagnetic d^4 species $Fe^{IV}Fe^{IV}$ and $Fe^{IV}O$ are made from **1a** and *t*-BuOOH in water;[4] they dominate at pH below and above 10, respectively. $Fe^{V}O$ is produced from **1a** and *m*-chloroperoxybenzoic acid at −40 °C in MeCN.[5] The Fe^{III} superoxo complex $Fe^{III}O_2$ was made from **1a** and KO_2 at 5 °C in MeCN.[40] By analyzing data from UV–vis, EPR, and Mössbauer spectra, we have been able to build a convincing case for the iron speciation of the reverse micellar media.

Studies of 1a in the Reverse Micelles by UV–vis Spectroscopy

In nonprotic organic solvents, the TAML activator **1a** is known to be oxidized by O_2 to the $Fe^{IV}Fe^{IV}$ dimer **2a**.[16] The oxidation does not occur in pure water. As introduced above, the overall water content in the system of AOT reverse micelles is much lower than in bulk water, which should increase the ratio of the O_2/H_2O exposure of **1a** and favor its oxidation. The first evidence for such oxidation was obtained by recording the UV–vis spectra of **1a** at variable pH (8–12) and degree of hydration w_0 (3–25). Complex **1a** does not absorb light above 600 nm. Thus, the observed buildup of broad bands in the range of 600–1100 nm in the AOT reverse micelles (Figure 2) was a reliable signal that iron(III) oxidation occurs in the presence of O_2.[4,16] The spectra obtained at w_0 3, 7, and 25 (pH 8) vary in the 600–1100 nm range, indicating that more than one species was formed and that the selectivity depends on w_0. The inset to Figure 2 shows that the species generated at w_0 3 were more stable than those at w_0 25.

Author Manuscript Author Manuscript Author Manuscript Author Manuscript

Spectra similar to those in Figure 2 were generated at pH 10 and 12 (see Figure S1 of SI). Oxidized iron species were produced in the AOT reverse micelles under all conditions studied but form slower at higher pH and higher w_0. Figures 2 and S1 (SI) allow for most of the known complexes to date to be labeled as likely or unlikely components of the reverse micellar media as explained next. The characteristic 360 nm band of **1a** was present under all studied conditions in the reverse micellar media. The species $Fe^{IV}Fe^{IV}$ and $Fe^{IV}O$ have been characterized previously[4] as products of the reaction between **1a** and *t*-BuOOH in water,[4] dominating at pH below and above 10, respectively. Both are diamagnetic EPR silent d^4 species, and their involvement in the speciation of the reverse micellar media is discussed in detail below. The UV–vis data provided evidence for the presence of $Fe^{IV}Fe^{IV}$ in the broad bands that can be observed at 800 and 1050 nm. The $Fe^{V}O$ complex was originally produced from **1a** and *m*-chloroperoxybenzoic acid at −40 °C in MeCN.[5] Prior experience suggests that $Fe^{V}O$ is unlikely to be stable under the conditions used herein.[18] The $Fe^{V}O$ complex in MeCN exhibits the characteristic UV–vis peak at 630 nm; there is no identifiable equivalent in Figure 2. Similarly, $Fe^{III}O_2$ made by Nam et al. from **1a** and KO_2 at 5 °C in MeCN was not present.[40] The UV–vis spectra were ambiguous regarding the presence of mononuclear $Fe^{IV}O$. However, Figures 2 and S1 (SI) make it clear that one or more additional species were present, as signified by the broad bands at 440 and 760 nm; these bands are suggestive of at least one novel dimer.

EPR Spectroscopy of 1a in the Reverse Micelles

The EPR spectra of **1a** ($Fe^{III}OH_2$) in water[23] and $Fe^{V}O$ in MeCN[5] have been characterized in earlier studies. The $Fe^{III}Fe^{IV}$ species of Chart 2 was previously unknown. The remaining species of Chart 2 are EPR silent. As stated above, the generation of $Fe^{III}O_2$ and $Fe^{V}O$ from **1a** and O_2 is improbable. The EPR spectrum of **1a** in the reverse micelles (pH 12) displayed a signal from the $Fe^{III}OH_2$ $S = 3/2$ species ($g = 4.0, 2.0$)[23] and a new previously unreported $S = 1/2$ species with $g = 1.99, 2.11, 2.14$ (Figure 3E). Similar EPR spectra were also recorded at pH 8 and 10 (Figure S2, SI). Spin quantification of the $S = 1/2$ species indicated that 15% of the initial concentration of **1a** converted to the $S = 1/2$ species. As shown below, the new species was assigned to heterovalent $Fe^{III}Fe^{IV}$ (Chart 2) or **3a** (Chart 1) and was also generated from **1a** and H_2O_2 in a buffered solution in the presence of glycerol.

EPR and Mössbauer Spectroscopy of 1a with H_2O_2

The EPR signal of **1a** ($Fe^{III}OH_2$) in phosphate buffer (pH 11.8) was extremely broad ($g = 4$, Figure 3A) due to intermolecular interaction. The addition of 50% glycerol to the solution significantly sharpened the EPR signal (Figure 3C). The simulation in Figure 3C (black line) for a spin $S = 3/2$ system includes a broad distribution of g values which was indicative of some aggregation in the presence of glycerol but significantly less than without glycerol. As in the glycerol-free system,[23] the temperature dependence of the signal indicates that the spectrum originates from a ground spin doublet with a positive zero-field splitting with $D = +2.5(5)\ cm^{-1}$. The signal intensity was in quantitative agreement with the amount of iron added to the solution.

The addition of 1 equiv of H_2O_2 to **1a** at room temperature and pH 11.8 generated a new EPR signal near $g = 2$ (Figure 3B) which was sharper in 50% glycerol (Figure 3D). The g

Author Manuscript Author Manuscript Author Manuscript Author Manuscript

values (1.992, 2.111 and 2.144) are indicative of a spin $S = 1/2$ system which matched the g values of the species observed in the reverse micelles without H_2O_2 (Figure 3E). In glycerol, the addition of H_2O_2 caused conversion of 60% of the initial amount of **1a** into other complexes. The amount of iron that converted into the $S = 1/2$ species accounted for 30% of the initial iron concentration of **1a**. The remainder (30% of the iron) converted to an EPR silent species, which is consistent with a previous report that peroxides convert Fe^{III} into an EPR-silent Fe^{IV} species.[4] Similar EPR samples were generated with ^{57}Fe-enriched **1a** and H_2O_2. Figure 4 shows an expanded scale of this species and $S = 1/2$ simulations. The broadening of the $g = 1.992$ peak (inset to Figure 4) was significant and was simulated with the addition of a hyperfine term for ^{57}Fe ($I = 1/2$) with $A = 18$ MHz. This value was in agreement with Mössbauer results shown below indicating that the $S = 1/2$ species was associated with iron.

TAML activators possess catalase-like activity[8] which causes evolution of O_2 due to the disproportionation of H_2O_2 at millimolar concentrations of **1a**. Therefore, the temperature was lowered to −20 °C (dry ice/acetone bath) prior to addition of H_2O_2 to slow the reaction. This increased the yield of the species, giving the $S = 1/2$ signal which was highest in the presence of 1 equiv of H_2O_2 but decreased at higher amounts of H_2O_2. The total iron concentration determined from quantification of the $S = 1/2$ and $S = 3/2$ EPR signals was significantly lower than total amount of iron introduced. However, as the initial concentration of **1a** was lowered, the percent yield of **3a** increased significantly (see Figure S3 of SI). At low **1a** concentration, and assuming the $S = 1/2$ signal is associated with a dinuclear iron complex, nearly quantitative yield of the $S = 1/2$ species was observed based on spin quantification. Furthermore, the Mössbauer spectra (see Figure 5 below) did not show a significant amount of mono- or dinuclear iron(IV) species under such conditions.

These results indicated that the $S = 1/2$ species was a heterovalent $Fe^{III}Fe^{IV}$ dimer. The Mössbauer data (Figure 5) confirmed the oxidation states as Fe^{III} and Fe^{IV}. The microwave saturation of the $S = 1/2$ signal was measured over the temperature range of 2 to 46 K. The half-power saturation data as a function of temperature was fit to an Orbach relaxation process (see Figure S5, SI), which determined the value of the exchange interaction between the Fe^{III} and Fe^{IV} centers, $J = -30 \pm 10$ cm^{-1}. There are a few characterized $Fe^{III}Fe^{IV}$ centers in model compounds[41–44] or proteins.[45,46] The exchange interactions for all of these previously characterized complexes were significantly larger in magnitude ($J < -100$ cm^{-1}). The exchange interaction for $Fe^{IV}Fe^{IV}$ species of TAML was also large ($J < -60$ cm^{-1}).[4] The lower exchange value for **3a** does not allow identification of a specific bridging species: the bridge could be oxo or hydroxo.

The spin quantification of **3a** allowed a determination of the extinction coefficients of the UV–vis spectral characteristics at ambient conditions. The UV–vis sample was prepared by adding 1 equiv of H_2O_2 to **1a** at pH 11.8 in 50% glycerol. The spectrum shown in Figure S4 (SI) did not change after 2 min needed for freezing EPR samples. The concentration of **3a** determined from the quantification of the EPR signal was used to calculate the extinction coefficients at 760 and 930 nm of 2500 and 425 M^{-1} cm^{-1}, respectively.

Author Manuscript Author Manuscript Author Manuscript Author Manuscript

The 4.2 K Mössbauer spectrum of **1a** enriched with ^{57}Fe at pH 11.8 in an applied magnetic field of 45 mT displayed a quadrupole doublet with $\delta = 0.14(4)$ mm s^{-1} and $\Delta E_Q = 3.97(4)$ mm s^{-1}. The absence of a magnetic splitting pattern indicated that **1a** was in the fast relaxation regime at 4.2 K. The Mössbauer spectrum in 50% glycerol (Figure 5A) was broad and remained broad at 140 K (Figure 5D), indicating an intermediate relaxation mode. The absence of a well resolved magnetic splitting pattern at 4.2 K was due to aggregation of **1a** in the aqueous environment, which was consistent with the EPR data.

The Mössbauer spectra at 4.2 and 140 K after the addition of 1 equiv of H_2O_2 to **1a** at pH 11.8 and −20 °C (50% glycerol) showed the partial loss of **1a** and the appearance of a new species (Figure 5B,E). The spectra of the new species (Figure 5C,F) were obtained by subtracting the corresponding spectra of **1a** (Figure 5A,C). The subtraction percentage (45% based on area) was determined by minimizing the features (indicated by arrows) attributed to **1a** in the 4.2 K spectrum. In agreement, the EPR spectra of samples prepared from the same stock solution as the Mössbauer samples showed the $S = 1/2$ and $S = 3/2$ signals at the same percentages in iron (assuming two irons per $S = 1/2$ species). As shown in Figure 5F, the spectrum was fit with two doublets of equal area with parameters $\delta = 0.01 \pm 4$, $\Delta E_Q = 3.09 \pm 5$ mm s^{-1} and $\delta = -0.11 \pm 4$, $\Delta E_Q = 3.33 \pm 5$ mm s^{-1}. These parameters could not be accurately determined from the spectra recorded at 4.2 K. The second-order Doppler correction would increase the isomer shift values by approximately +0.06 mm s^{-1}. Previously characterized mononuclear Fe^{III} macrocyclic complexes have δ and ΔE_Q in the range of 0.12 to 0.25 mm s^{-1} and 3.6 to 4.19 mm s^{-1}, respectively.[47–49] The δ and ΔE_Q values for similar Fe^{IV} complexes are −0.19 to −0.03 mm s^{-1} and 0.89 to 4.35 mm s^{-1}, respectively.[4,16,50,51] Including the correction, the isomer shifts of +0.07 mm s^{-1} and −0.05 mm s^{-1} from **3a** are close to or in range of the isomer shifts from the previously characterized Fe^{III} and Fe^{IV} complexes, respectively.

The Mössbauer spectra of **3a** recorded in the magnetic fields of 0.05, 3, and 8 T are shown in Figure 6. The sample was prepared as in Figure 5, and the spectra are displayed after subtraction of 45% of the corresponding spectra of **1a** (based on area). Raw spectra are shown in Figure S6, SI. The spectra were simulated using eq 1 for an antiferromagnetic exchange of $J = -30$ cm^{-1} between the Fe^{III} and Fe^{IV} sites as determined above from EPR spectroscopy. The agreement of Mössbauer spectra with simulations indicate that the spin states of the Fe^{III} and Fe^{IV} sites are $S = 3/2$ and 1, respectively. These spin states are the same as those observed for monomeric Fe^{III} or Fe^{IV} TAML complexes characterized previously.[4,23] The simulations use a set of parameters for D, E/D, and **A**-tensors given in the figure caption that are derived from least-squares fits of the data. The parameters set was not unique but was consistent with the spin state assignments.

Speciation of Iron in Reverse Micelles

EPR and Mössbauer studies of **1a**/H_2O_2 in 50% glycerol allowed identification of the Fe^{III}Fe^{IV} (**3a**) species formed from **1a** and O_2 in the reverse micelles. The plausible coexisting species are Fe^{III}OH$_2$, Fe^{III}Fe^{IV}, Fe^{IV}Fe^{IV}, and Fe^{IV}O (Chart 2). In water, Fe^{IV}Fe^{IV} and Fe^{IV}O exist in a pH-controlled equilibrium.[4] The former dominates at pH < 10, the latter at pH > 12. It is important to note that the effective pH in the AOT reverse

Author Manuscript Author Manuscript Author Manuscript Author Manuscript

micelles may differ from the pH of the aqueous buffer introduced (and indicated throughout). The acidity can be higher near the interface for negatively charged surfactants.[52] The effective pH is usually lower by 1–3 units in the AOT reverse micelles than in the bulk water depending on w_0,[53,54] though the difference may be smaller than 1 unit when w_0 is high.[28] Therefore, $Fe^{IV}O$ cannot be a dominating species and probably does not form at all. The absence of the peak around 435 nm in Figures 2 and S1, which is typical of $Fe^{IV}O$ (ε = 2500 M^{-1} cm^{-1}),[4] gives additional evidence. Thus, the remaining species to be considered are $Fe^{III}OH_2$, $Fe^{III}Fe^{IV}$, and $Fe^{IV}Fe^{IV}$. The latter has a sharper band at 481 nm and a broader band at 856 nm, whereas the band at 365 nm is weaker as compared to that of $Fe^{III}OH_2$. The less oxidized $Fe^{III}Fe^{IV}$ has two bands at 440 and 760 nm. These bands allowed semiquantitative interpretation from the spectral data in the range of 760–930 nm where $Fe^{III}OH_2$ does not absorb. The estimations were obtained using eqs 3 and 4 that connect absorbances at 760 and 930 nm to concentrations of the iron dimers using the known values of ε_{760} and ε_{930} (2500 and 425 M^{-1} cm^{-1} for $Fe^{III}Fe^{IV}$ vs 4820 and 3056 M^{-1} cm^{-1} for $Fe^{IV}Fe^{IV}$, respectively). We assumed that the extinction coefficients were approximately independent of w_0 and pH.

$$A_{760}=2500[\mathrm{Fe^{III}Fe^{IV}}]+4820[\mathrm{Fe^{IV}Fe^{IV}}] \quad (3)$$

$$A_{930}=425[\mathrm{Fe^{III}Fe^{IV}}]+3056[\mathrm{Fe^{IV}Fe^{IV}}] \quad (4)$$

The amount of $Fe^{III}OH_2$ shown in Figure 7 was obtained by subtracting 2 × [$Fe^{III}Fe^{IV}$] and 2 × [$Fe^{IV}Fe^{IV}$] from the total iron in the system. $Fe^{III}OH_2$ dominates under almost all conditions tested, i.e., there is incomplete oxidation of Fe^{III} by O_2 in the reverse micellar media under the conditions studied. The more heterovalent dimer $Fe^{III}Fe^{IV}$, the major Fe^{IV}-containing material, is formed at higher pH and moderate w_0, consistent with the fact that basic conditions stabilize $Fe^{III}Fe^{IV}$ in aqueous glycerol. The homovalent dimer is present at low w_0 and pH 8 because aprotic organic medium and this pH are both favorable for $Fe^{IV}Fe^{IV}$.[4,16] The Fe^{IV} percentage drops at higher w_0 because “wet” micelles are closer to bulk water where **1a** is not oxidized by O_2.[16]

The data in Figure 7 should be considered as qualitative because water inside reverse micelles is dissimilar to bulk water in terms of polarity, acidity, and microscopic viscosity.[24,54] As a result, the environment of **1a** varies with the degree of hydration w_0 of the reverse micelles, and the ε values in reverse micelles and pure water may differ. Nevertheless, estimates in Figure 7 for the UV–vis data agree with the EPR results in Figures 3 and S2 (SI) because the spin quantitation gives the yields of $Fe^{III}Fe^{IV}$ of 13, 33, and 37% at pH 8, 10, and 12, respectively, at w_0 10 and total iron of 1.5 × 10^{-4} M. Thus, **1a** is oxidized in the O_2-rich system into Fe^{IV} species in the absence of peroxides. We will now describe the catalytic activation of O_2 by **1a** in these reverse micelles.

Author Manuscript Author Manuscript Author Manuscript Author Manuscript

Catalytic Oxidation of NADH in Reverse Micelles

The NADH/NAD^+ couple is the essence of numerous biological processes[55–57] including those catalyzed by NAD^+-dependent dehydrogenases, viz. enzymes that are widely used in organic synthesis.[56,58] The limitations of enzymatic processes are due to the cost of NAD^+,[59] and therefore reliable systems for NAD^+ regeneration are needed, as the current methods are still not adequately effective.[60] TAMLs catalyze the oxidation of NADH by enzymatically produced H_2O_2 under mild conditions,[61] and therefore NADH was the first choice substrate.

Smooth conversion of NADH into NAD^+ catalyzed by **1a**/O_2 was monitored by UV–vis spectroscopy at 340 nm (maximum for NADH; NAD^+ does not absorb) at w_0 in the range of 3 to 25 and pH 8, 10, and 12. At pH 10 the isosbestic point holds at 286 nm (Figure 8A). Control experiments in the reverse micelles in the absence of **1a** showed negligible oxidation of NADH within the same time period (Figure S7, SI). The catalytic conversion of NADH into NAD^+ rather than into smaller fragments was proven by HPLC[38] by comparing the elution times of the product and authentic NAD^+. At pH 10 and w_0 10, no NADH was observed after 9 h by UV–vis spectroscopy when the spectra were recorded every 30 s (see below for explanations). The 83% yield of NAD^+ was calculated from the HPLC data. This corresponds to the turnover number (TON) of 88 and turnover frequency (TOF) of 0.003 s^{-1} at [**1a**] = 2.46×10^{-6} M and [NADH] = 2.6×10^{-4} M. The control experiment in the absence of **1a** showed 67% NADH and 27% NAD^+ by HPLC after 9 h. Catalyst **1a** converts NADH into the “enzymatically active” NAD^+. Alcohol dehydrogenase (ADH) and ethanol rapidly reduce NAD^+ formed to NADH,[60] and 95% NADH reappears almost instantly, much faster than the NADH oxidation (inset to Figure 8B). These results lead to the conclusion that the oxidation proceeds according to eq 5.

$$\mathrm{NADH} + \frac{1}{2}\mathrm{O_2} + \mathrm{H^+} \xrightarrow{\mathrm{TAML}} \mathrm{NAD^+} + \mathrm{H_2O} \quad (5)$$

Whenever the catalytic reduction of O_2 is being studied, it is important to be sure that adventitious oxidizing agents are not interfering with the reaction chemistry.[62] A major concern is the presence of peroxidic impurities in the components of the reaction media. To rule out the possible involvement of peroxides, **1b**, which is more reactive in oxidations by H_2O_2 in pure water than **1a**,[8] was used as the catalyst in the reverse micellar oxidation of NADH. Fluorinated TAMLs such as **1b** react with O_2 in aprotic solvents much slower than their methylated counterparts.[16] The data in Figure S8 (SI) show that **1b** is 5-times less reactive than **1a** in the reverse micelles at pH 10 and w_0 3. This establishes that adventitious peroxides are unlikely major participants. Furthermore, colorimetric testing for peroxide with KI and peroxide test strips produce no color changes.[37] These results support the case that **1a** does indeed launch an oxygenase-like process eq 5 in the reverse micelles and that H_2O_2 is not involved.

Next the ability of the iron(IV) complex **2a**[16] to oxidize NADH ([Fe^{IV}]:[NADH] = 1:1.05) was tested in reverse micelles in degassed media under argon to preclude or at least minimize autoxidation. The NADH absorbance around 340 nm decreased on addition of **2a**,

Author Manuscript Author Manuscript Author Manuscript Author Manuscript

indicative of the oxidation of NADH (Figure 9). NAD^+ was produced in 62 and 52% with respect to the total iron according to UV–vis and HPLC data, respectively. When ferric **1a** was employed in place of **2a** under otherwise identical conditions, the yield of NAD^+ fell to 14% (HPLC). That any oxidation was observed at all suggested that O_2 was not excluded completely by the degassing procedure. These facts support the hypothesis that NADH can be oxidized by **2a** and allow us to conclude that catalyst-based oxidations are competent to produce the observed chemistry in these reaction systems where one should always be on the lookout for adventitious free radical autoxidation.

Comparison of Initial Rates of NADH Oxidation

NADH is slowly oxidized in reverse micelles in the absence of **1a** as shown in Figure S7 (SI). TAML **1a** accelerates the oxidation to such extent that the spontaneous process can be neglected in many cases. Nevertheless, the initial rates shown in 3D Figure 10 were corrected for the uncatalyzed reaction in the absence of **1a**. The degree of hydration w_0 is a key factor that regulates the reactivity. Reaction 5 is strikingly faster in lower w_0 micelles. One explanation is that water impedes the binding of O_2 to the Fe^{III} center thus slowing the catalytic rate. However, the actual concentrations of iron species and/or NADH within a microreactor will be changing with w_0. The catalyst will certainly partition preferentially to the water, so concentration effects cannot be neglected and perhaps provide the dominant explanation.[63] Reaction 5 is much less sensitive to pH than to w_0 (Figure 10).

Effect of Light on the Catalyzed NADH Oxidation in Reverse Micelles

TAML-catalyzed reaction 5 is accelerated by light. The effect was established by changing the scanning frequency when the NADH oxidation was monitored by a photodiode array UV–vis spectrometer. The process was noticeably faster when spectra were registered more frequently, i.e., when the flash frequency (F_f = inverse time between recording (TbR) of successive spectra) was higher (Figure 11). The slowest rate was registered when reaction 5 was followed using a double beam UV–vis spectrometer, but it increased *linearly* with increasing flash frequency when the photodiode array instrument was used (inset to Figure 11). The straight line has an insignificant positive intercept which may reflect a dark process. A double beam spectrometer emits much less light to the sample than a photodiode array instrument which utilizes the undispersed light beam in the 190–1100 nm spectral region. Reactions susceptible to “diode array acceleration” are known and have recently been reviewed.[64] The majority of these processes involve O_2. The mechanisms do not involve species in long-lived excited states and are usually complex requiring individual systematic studies.

The light accelerates the uncatalyzed oxidation of NADH in the reverse micelles in the absence of **1a** (Figure S7, SI). Thus, the irradiation affects NADH. Experiments with pinacyanol chloride (Figure S9, SI) suggest that irradiation does not impact **1a** directly. The bleaching rate of PNC was found to be practically insensitive to the flash frequency of the photodiode array spectrometer (Figure S9, SI); a minor effect is ascribed to the reported photodegradation of aggregated PNC in water,[65] which is also observed in the absence of **1a** (inset to Figure S9, SI). The kinetics of absorbance growth at 750 nm has been studied to probe the formation of $Fe^{III}Fe^{IV}$ and/or $Fe^{IV}Fe^{IV}$ from **1a** and O_2 in the reverse micelles as a

Author Manuscript Author Manuscript Author Manuscript Author Manuscript

function of the flash frequency at w_0 15 and pH 12. Under such conditions the rates are lower and the measurements are more accurate. No light effect was registered (see Figure S10, SI), indicating that NADH is the photosensitive component of reaction 5.

Oxidation of Pinacyanol Chloride and Hydroquinone

In 1998, PNC was used to unveil the catalytic activity of **1a**/H_2O_2.[66] PNC has limited solubility in aqueous buffer at pH 12 but dissolves readily in the AOT reverse micelles. As noted above, PNC decomposes slowly in the reverse micelles without **1a** (Figure S9, SI); the process is faster in water at pH 10 due to the aggregation of PNC to form a dark solid.[67] The oxidation of PNC by O_2 in the reverse micelles is strongly catalyzed by **1a** at pH 10 (Figures 12 and S9, SI). The bleaching of PNC was investigated in some detail at w_0 3, 10, and 25 and pH 8, 10, and 12 (Table S4, SI). It is rather slow at pH 8 typical of lower activity of **1a**/H_2O_2 in water at neutral/acidic pHs.[3] At pH 10, the fastest bleaching was observed at w_0 10, but it slowed down in the "drier micelles" at w_0 3 (Figure S11, SI). The oxidation of Fe^{III} to Fe^{IV} and the oxidative bleaching of PNC by Fe^{IV} are affected oppositely by w_0. Lower w_0 values favor the former process but disfavor the latter. Under the optimal conditions (w_0/pH = 10/12) in the presence of just 1% **1a**, TON and TOF equal 90 and 1.6 × 10^{-3} s^{-1}, respectively. The **1a**-catalyzed oxidation of PNC by O_2 in the reverse micelles is less deep than by H_2O_2 in water. Figure 12 shows that a decrease of the main 600 nm peak is accompanied by a buildup of a smaller peak at 350 nm, which was not observed in the aqueous solution.[68]

The rapid oxidation of hydroquinone (λ_{max} 289 nm) to 1,4-benzoquinone (λ_{max} 247 nm)[69] is conveniently studied by UV–vis spectroscopy.[69] The process is very fast under basic conditions and is followed by a second oxidation step.[70] The spontaneous oxidation of HQ was found to slow in the reverse micelles prepared using a tiny amount of water (w_0 ~1.6, see Experimental Section) and studied immediately after preparation. The oxidation of HQ is faster in the presence of **1a** under all conditions tested. Notably, the HQ oxidation was faster in wet micelles with higher w_0 (Figure S13, SI), in contrast with the oxidation of NADH, which was found to be more rapid in micelles with low w_0, or PNC, which occurred most rapidly at intermediate w_0. This is probably because the effective pH inside the water pools decreases with w_0 to favor HQ stability. A secondary oxidation process is also visible for HQ at higher pH (pH 10 and 12, Figure S12, SI).

Limitations of Reverse Micelles as Media for TAML-Catalyzed Oxidation by O_2

TAML activators catalyze the bleaching of Orange II[7] and Safranin O[71] dyes by H_2O_2 in water. These two dyes are more difficult to decolorize than PNC.[68] Orange II has become widely used for assaying the catalytic activity of synthetic oxidation catalysts.[7,11,30,72–74] Neither Orange II nor Safranin O were decolorized in the presence of **1a** in the AOT reverse micelles even in the presence of equimolar amounts of **1a** and Orange II or Safranine O in the reaction media.

Author Manuscript Author Manuscript Author Manuscript Author Manuscript

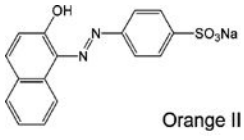

Orange II

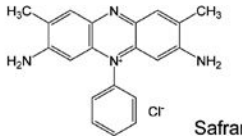

Safranin O

On the Formation of the Heterovalent Dimer

The AOT reverse micelle microreactors have proven to be attractive and challenging media for TAML activator processes. By imposing limitations on the water content of the AOT microreactors to favor TAML interactions with O_2 in the adjacent dioxygen pool, the resting ferric species is easily converted into iron(IV) derivatives that can catalytically oxidize selected electron donors. These oxidations replace H_2O_2 as a primary oxidant of TAML catalysis with the far more technically attractive O_2. In the reverse micelles, O_2 converts iron(III) TAML **1a** into the heterovalent $Fe^{III}Fe^{IV}$ dimer **3a** via the simplified process of eq 6, assuming the μ-oxo bridged formulation. There are relatively few characterized $Fe^{III}Fe^{IV}$ centers in synthetic complexes[41–44,75–77] and metalloproteins,[45,46,78,79] and this adds interest to the discovery of compound **3a**. The reaction stoichiometry is rather unusual for iron–oxygen interactions[80,81] because one O_2 molecule formally requires eight iron(III) units for complete depositing its four electrons.

$$8[Fe^{III}OH_2]^- + O_2 \rightarrow 4[Fe^{IV}OFe^{IV}]^{3-} + 6H_2O + 4H^+ \quad (6)$$

$$4[Fe^{III}OH_2]^- + O_2 \rightarrow 2[Fe^{IV}OFe^{IV}]^{2-} + 4H_2O \quad (7)$$

Equation 6 should be compared with the known process of eq 7 in which iron(III) TAML activators are rapidly oxidized by O_2 in aprotic organic solvents to form the homovalent $Fe^{IV}Fe^{IV}$ μ-oxo bridged dimer **2a**.[16] In this case, four iron(III) units are needed, which is of course, a more common scenario.[82] Hydrogen peroxide as a 2e oxidant leads to **3a** via eq 8, i.e., the iron(III) to H_2O_2 stoichiometry is 4:1 at pH 11.8 in 50% glycerol at lower temperatures.

$$4[Fe^{III}OH_2]^- + H_2O_2 \rightarrow 2[Fe^{III}OFe^{IV}]^{3-} + 4H_2O + 2H^+ \quad (8)$$

It is intriguing that the yield of **3a** produced in pure water is much lower than in the presence of glycerol; the dominant product in pure water is the homovalent dimer **2a**.[4] Explanations are conceivable. For example, glycerol may be more than a cosolvent[83] by behaving as a reducing agent[84,85] to favor the formation of the less oxidized heterovalent dimer **3a**.

Reactivity Comparisons of TAML Species

The oxygenase-like activity of TAML activators in the reverse micelles established in this work is moderate; **1a**/O_2 does not bleach what are facile targets in water, such as Orange II, but does catalyze the mild oxidation of reactive electron donors such as NADH;

Author Manuscript Author Manuscript Author Manuscript Author Manuscript

enzymatically active NAD^+ is produced with TON of 88. The TOF of 0.003 is, however, lower than those recently reported for O_2 oxidations involving the iron(III) complex of *meso*-tetrakis(4-sulfonatophenyl)porphyrin (0.11 in the aqueous phosphate buffer of pH 7)[86] and **1a** in the presence of glucose oxidase/D-glucose (ca. 0.03 at pH 7.5).[61]

The lower reactivity of **1a** in these reverse micelles may have advantages. Typically, TAML activators in basic water catalyze multistep, deep oxidation of organic substrates by H_2O_2,[17] fragmenting and nearly mineralizing persistent pollutants including polychlorophenols,[87] organophosphorus pesticides,[88] and many others.[17] Here the mild process for NADH, even with light induction, is reminiscent of cellular processes where the NAD^+ is available for catalytic cycling. Thus, the activity achieved may be of use for transformations of fragile molecules by O_2 that avoid destructive deep oxidation. We are further examining the potential.

The lower reactivity of TAML activators in these processes is adequately understood at a molecular level because there is a clear parallel between the reactivity and the iron oxidation state as shown in Chart 2 where the iron oxidation state in characterized TAML species increases from left to right (from 3+ to 5+); $Fe^{V}O$ expresses a ca. 10^4 fold rate advantage over $Fe^{IV}Fe^{IV}$ in organic media.[18,19] Monomers $Fe^{IV}O$ are known to be more reactive than dimers $Fe^{IV}Fe^{IV}$ in aqueous solutions.[89] Thus, the dominating speciation of iron here as the least oxidized and oxidizing $Fe^{III}Fe^{IV}$ explains the observed reactivity picture.

CONCLUSIONS

By catalyzing the oxidation of NADH to NAD^+ by O_2 in AOT reverse micelles with a TON of 88, peroxidase-mimicking TAML activators have been shown to be capable of oxygenase-mimicry under appropriately engineered conditions. The oxygen oxidations are less aggressive than hydrogen peroxide oxidations. Nevertheless, oxygen is special, making the findings important and suggesting that more research should be carried out to explore whether or not TAML activators can function effectively using affordable molecular oxygen in a wide range of oxidation processes.

Supplementary Material

Refer to Web version on PubMed Central for supplementary material.

Acknowledgments

T.J.C. thanks the Heinz endowments for support of the Institute for Green Science which covered this study. M.P.H. acknowledges funding from National Institute of Health grant R01 GM077387. Funding for the EPR spectrometer is from National Science Foundation grant CHE1126268.

References

1. Collins T. J Acc Chem Res. 2002; 35:782–790.
2. Collins, TJ., Khetan, SK., Ryabov, AD. Handbook of Green Chemistry. Anastas, PT., Crabtree, RH., editors. Wiley-VCH Verlag GmbH & Co. KgaA; Weinheim: 2009. p. 39-77.
3. Ryabov AD, Collins TJ. Adv Inorg Chem. 2009; 61:471–521.

Author Manuscript Author Manuscript Author Manuscript Author Manuscript

4. Chanda A, Shan X, Chakrabarti M, Ellis W, Popescu D, Tiago de Oliveira F, Wang D, Que L Jr, Collins TJ, Münck E, Bominaar EL. Inorg Chem. 2008; 47:3669–3678. [PubMed: 18380453]
5. Tiago de Oliveira F, Chanda A, Banerjee D, Shan X, Mondal S, Que L Jr, Bominaar EL, Münck E, Collins TJ. Science. 2007; 315:835–838. [PubMed: 17185561]
6. Dunford, HB. Heme Peroxidases. Wiley-VCH; New York: 1999.
7. Chahbane N, Popescu D-L, Mitchell DA, Chanda A, Lenoir D, Ryabov AD, Schramm K-W, Collins TJ. Green Chem. 2007; 9:49–57.
8. Ghosh A, Mitchell DA, Chanda A, Ryabov AD, Popescu DL, Upham E, Collins GJ, Collins TJ. J Am Chem Soc. 2008; 130:15116–15126. [PubMed: 18928252]
9. Popescu D-L, Chanda A, Stadler MJ, Mondal S, Tehranchi J, Ryabov AD, Collins TJ. J Am Chem Soc. 2008; 130:12260–12261. [PubMed: 18722448]
10. Ellis WC, Tran CT, Denardo MA, Fischer A, Ryabov AD, Collins TJ. J Am Chem Soc. 2009; 131:18052–18053. [PubMed: 19928965]
11. Ellis WC, Tran CT, Roy R, Rusten M, Fischer A, Ryabov AD, Blumberg B, Collins TJ. J Am Chem Soc. 2010; 132:9774–9781. [PubMed: 20565079]
12. Jones, CW. Applications of hydrogen peroxide and derivatives. The Royal Society of Chemistry; Cambridge: 1999.
13. Stahl, SS., Lippard, SJ. Iron Metabolism. Ferreira, GC.Moura, JJG., Franco, R., editors. Wiley-VCH; Weinheim: 1999. p. 303-321.
14. Bakač A. Inorg Chem. 2010; 49:3584–3593. [PubMed: 20380460]
15. Campbell AN, Stahl SS. Acc Chem Res. 2012; 45:851–863. [PubMed: 22263575]
16. Ghosh A, Tiago de Oliveira F, Yano T, Nishioka T, Beach ES, Kinoshita I, Münck E, Ryabov AD, Horwitz CP, Collins TJ. J Am Chem Soc. 2005; 127:2505–2513. [PubMed: 15725005]
17. Ryabov AD. Adv Inorg Chem. 2013; 65:118–163.
18. Kundu S, Van Kirk Thompson J, Ryabov AD, Collins TJ. J Am Chem Soc. 2011; 133:18546–18549. [PubMed: 21985217]
19. Kundu S, Thompson JVK, Shen LQ, Mills MR, Bominaar EL, Ryabov AD, Collins TJ. Chem – Eur J. 2015; 21:1803–1810. [PubMed: 25410933]
20. Ghosh M, Singh KK, Panda C, Weitz A, Hendrich MP, Collins TJ, Dhar BB, Sen Gupta S. J Am Chem Soc. 2014; 136:9524–9527. [PubMed: 24387595]
21. Panda C, Debgupta J, Diaz Diaz D, Singh KK, Sen Gupta S, Dhar BB. J Am Chem Soc. 2014; 136:12273–12282. [PubMed: 25119524]
22. Kwon E, Cho K-B, Hong S, Nam W. Chem Commun. 2014; 50:5572–5575.
23. Ghosh A, Ryabov AD, Mayer SM, Horner DC, Prasuhn DE Jr, Sen Gupta S, Vuocolo L, Culver C, Hendrich MP, Rickard CEF, Norman RE, Horwitz CP, Collins TJ. J Am Chem Soc. 2003; 125:12378–12378. [PubMed: 14531659]
24. Fendler JH. Acc Chem Res. 1976; 9:153–61.
25. Pileni MP. J Phys Chem. 1993; 97:6961–73.
26. Levashov, AV., Klyachko, NL., editors. Enzymes in reverse micelles (microemulsions): Theory and practice. Marcel Dekker Inc; New York: 2003.
27. La Sorella G, Strukul G, Scarso A. Green Chem. 2015; 17:644–683.
28. De TK, Maitra A. Adv Colloid Interface Sci. 1995; 59:95–193.
29. Stadler, MJ. Ph.D. Thesis. Carnegie Mellon University; Pittsburgh, PA: 2007.
30. Banerjee D, Apollo FM, Ryabov AD, Collins TJ. Chem -Eur J. 2009; 15:10199–10209. [PubMed: 19711381]
31. Battino R, Rettich TR, Tominaga T. J Phys Chem Ref Data. 1983; 12:163–178.
32. Biasutti MA, Abuin EB, Silber JJ, Correa NM, Lissi EA. Adv Colloid Interface Sci. 2008; 136:1–24. [PubMed: 17706582]
33. Ellis, WC. Ph.D. Thesis. Carnegie Mellon University; Pittsburgh, PA: 2010.
34. Ghosh, A. Ph D Thesis. Carnegie Mellon University; Pittsburgh, PA: 2004.
35. George P. Biochem J. 1953; 54:267–276. [PubMed: 13058869]
36. Menger FM, Yamada K. J Am Chem Soc. 1979; 101:6731–6734.

Author Manuscript Author Manuscript Author Manuscript Author Manuscript

37. Carroll, WFJ., Foster, BL., Barkley, WE., Cook, SH., Fivizzani, KP., Izzo, R., Jacobson, KA., Maupins, K., Moloy, K., Ogle, RB., Palassis, J., Phifer, RW., Reinhardt, PA., Thompson, LT., Winfield, L. Prudent Practices in the Laboratory. The National Academies Press; Washington, D.C.: 2011.
38. Markham KA, Kohen A. Curr Anal Chem. 2006; 2:379–388.
39. Petasis, DT., Hendrich, MP. Quantitative interpretation of EPR spectroscopy with applications for iron-sulfur proteins. Rouault, TA., editor. De Gruyter; Berlin: 2014. p. 21-48.
40. Hong S, Sutherlin KD, Park J, Kwon E, Siegler MA, Solomon EI, Nam W. Nat Commun. 2014; 5:5440. [PubMed: 25510711]
41. Dong Y, Que L Jr, Kauffmann K, Münck E. J Am Chem Soc. 1995; 117:11377–11378.
42. Lee D, Du Bois J, Petasis D, Hendrich MP, Krebs C, Huynh BH, Lippard SJ. J Am Chem Soc. 1999; 121:9893–9894.
43. Lee D, Pierce B, Krebs C, Hendrich MP, Huynh BH, Lippard SJ. J Am Chem Soc. 2002; 124:3993–4007. [PubMed: 11942838]
44. Slep LD, Mijovilovich A, Meyer-Klaucke W, Weyhermueller T, Bill E, Bothe E, Neese F, Wieghardt K. J Am Chem Soc. 2003; 125:15554–15570. [PubMed: 14664603]
45. Sturgeon BE, Burdi D, Chen S, Huynh B-H, Edmondson DE, Stubbe J, Hoffman BM. J Am Chem Soc. 1996; 118:7551–7557.
46. Valentine AM, Tavares P, Pereira AS, Davydov R, Krebs C, Hoffman BM, Edmondson DE, Huynh BH, Lippard SJ. J Am Chem Soc. 1998; 120:2190–2191.
47. Kostka KL, Fox BG, Hendrich MP, Collins TJ, Rickard CEF, Wright LJ, Münck E. J Am Chem Soc. 1993; 115:6746–6757.
48. Bartos MJ, Kidwell C, Kauffmann KE, Gordon-Wylie SW, Collins TJ, Clark GC, Münck E, Weintraub ST. Angew Chem, Int Ed Engl. 1995; 34:1216–19.
49. Bartos MJ, Gordon-Wylie SW, Fox BG, Wright LJ, Weintraub ST, Kauffmann KE, Münck E, Kostka KL, Uffelman ES, Rickard CEF, Noon KR, Collins TJ. Coord Chem Rev. 1998; 174:361–390.
50. Collins TJ, Kostka KL, Münck E, Uffelman ES. J Am Chem Soc. 1990; 112:5637–5639.
51. Collins TJ, Fox BG, Hu ZG, Kostka KL, Münck E, Rickard CEF, Wright LJ. J Am Chem Soc. 1992; 114:8724–5.
52. Biasutti MA, Abuin EB, Silber JJ, Correa NM, Lissi EA. Adv Colloid Interface Sci. 2008; 136:1–24. [PubMed: 17706582]
53. Grandi C, Smith RE, Luisi PL. J Biol Chem. 1981; 256:837–843. [PubMed: 7192710]
54. Shield JW, Ferguson HD, Bommarius AS, Hatton TA. Ind Eng Chem Fundam. 1986; 25:603–612.
55. Pollak N, Dolle C, Ziegler M. Biochem J. 2007; 402:205–218. [PubMed: 17295611]
56. Gamenara, D., Seoane, G., Saenz-Méndez, P., Domínguez de María, P. Redox Biocatalysis: Fundamentals and Applications. Wiley; Hoboken, NJ: 2013.
57. Uppada V, Bhaduri S, Noronha SB. Curr Sci. 2014; 106:946–957.
58. Weckbecker A, Groger H, Hummel W. Adv Biochem Eng /Biotechnol. 2010; 120:195–242.
59. Wichmann R, Vasic-Racki D. Adv Biochem Eng /Biotechnol. 2005; 92:225–260.
60. Golub E, Freeman R, Willner I. Angew Chem, Int Ed. 2011; 50:11710–11714.
61. Miller JA, Alexander L, Mori DI, Ryabov AD, Collins TJ. New J Chem. 2013; 37:3488–3495.
62. Scheeline A, Olson DL, Williksen EP, Horras GA, Klein ML, Larter R. Chem Rev. 1997; 97:739–756. [PubMed: 11848887]
63. Berezin IV, Martinek K, Yatsimirskii AK. Russ Chem Rev. 1973; 42:1729–1756.
64. Fabian I, Lente G. Pure Appl Chem. 2010; 82:1957–1973.
65. Byers GW, Gross S, Henrichs PM. Photochem Photobiol. 1976; 23:37–43. [PubMed: 1265127]
66. Horwitz CP, Fooksman DR, Vuocolo LD, Gordon-Wylie SW, Cox NJ, Collins TJ. J Am Chem Soc. 1998; 120:4867–4868.
67. Khouri SJ, Buss V. J Solution Chem. 2010; 39:121–130.
68. Mitchell DA, Ryabov AD, Kundu S, Chanda A, Collins TJ. J Coord Chem. 2010; 63:2605–2618.
69. Li YB, Trush MA. Arch Biochem Biophys. 1993; 300:346–355. [PubMed: 8424668]

Author Manuscript Author Manuscript Author Manuscript Author Manuscript

70. James TH, Snell JM, Weissberger A. J Am Chem Soc. 1938; 60:2084–2093.
71. Chanda A, Ryabov AD, Mondal S, Alexandrova L, Ghosh A, Hangun-Balkir Y, Horwitz CP, Collins TJ. Chem – Eur J. 2006; 12:9336–9345. [PubMed: 17029311]
72. Theodoridis A, Maigut J, Puchta R, Kudrik EV, Van Eldik R. Inorg Chem. 2008; 47:2994–3013. [PubMed: 18351731]
73. Ember E, Rothbart S, Puchta R, van Eldik R. New J Chem. 2009; 33:34–49.
74. Rothbart S, Ember EE, van Eldik R. New J Chem. 2012; 36:732–748.
75. Voronkova VK, Mrozinski J, Yampol'skaya MA, Yablokov YV, Evtushenko NS, Byrke MS, Gerbeleu NV. Inorg Chim Acta. 1995; 238:139–147.
76. Korendovych IV, Kryatov SV, Rybak-Akimova EV. Acc Chem Res. 2007; 40:510–21. [PubMed: 17521158]
77. Goure E, Avenier F, Dubourdeaux P, Seneque O, Albrieux F, Lebrun C, Clemancey M, Maldivi P, Latour J-M. Angew Chem, Int Ed. 2014; 53:1580–4.
78. Voevodskaya N, Galander M, Hogbom M, Stenmark P, McClarty G, Graslund A, Lendzian F. Biochim Biophys Acta, Proteins Proteomics. 2007; 1774:1254–1263.
79. Voevodskaya N, Lendzian F, Graslund A. Biochem Biophys Res Commun. 2005; 330:1213–1216. [PubMed: 15823572]
80. Bertini, I., Gray, HB., Lippard, SJ., Valentine, JS. Bioinorganic Chemistry. University Science Books; Mill Valley, CA: 1994.
81. Bertini, I., Gray, HB., Stiefel, EI., Valentine, JS. Biological Inorganic Chemistry Structure and Reactivity. University Science Books; Sausalito, CA: 2007.
82. Kryatov SV, Rybak-Akimova EV, Schindler S. Chem Rev. 2005; 105:2175–2226. [PubMed: 15941212]
83. Chahdoura F, Favier I, Gómez M. Chem – Eur J. 2014; 20:10884–10893. [PubMed: 25069778]
84. Mandelli D, Carvalho WA, Shul'pina LS, Kirillov AM, Kirillova MV, Pombeiro AJL, Shul'pin GB. Adv Organomet Chem Catal. 2014:247–257.
85. Katryniok B, Kimura H, Skrzynska E, Girardon J-S, Fongarland P, Capron M, Ducoulombier R, Mimura N, Paul S, Dumeignil F. Green Chem. 2011; 13:1960–1979.
86. Maid H, Böhm P, Huber SM, Bauer W, Hummel W, Jux N, Gröger H. Angew Chem, Int Ed. 2011; 50(2397–2400):2397–2400.
87. Gupta SS, Stadler M, Noser CA, Ghosh A, Steinhoff B, Lenoir D, Horwitz CP, Schramm K-W, Collins TJ. Science. 2002; 296:326–328. [PubMed: 11951040]
88. Chanda A, Khetan SK, Banerjee D, Ghosh A, Collins TJ. J Am Chem Soc. 2006; 128:12058–12059. [PubMed: 16967942]
89. Banerjee D, Ryabov AD, Collins TJ. J Coord Chem. 2015; :68.doi: 10.1080/00958972.2015.1065974

Author Manuscript Author Manuscript Author Manuscript Author Manuscript

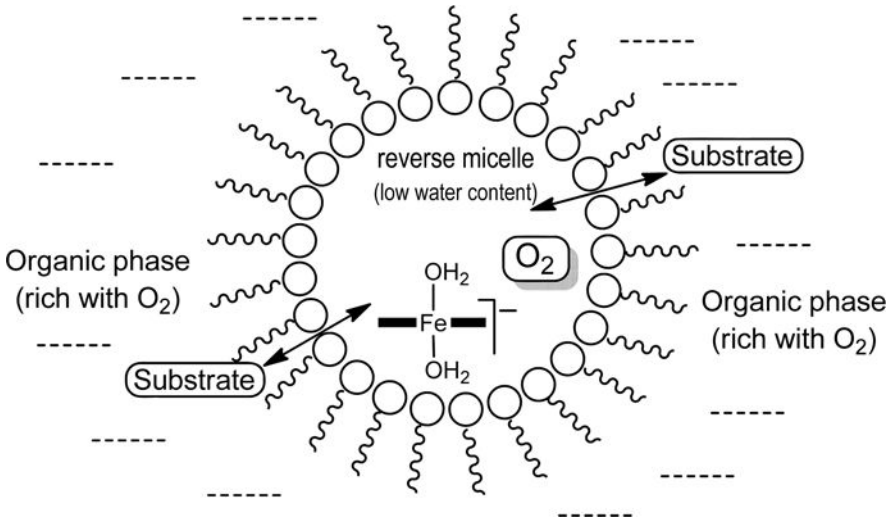

Figure 1.
Schematic drawing of the reverse micelle incorporating TAML activators.

Author Manuscript Author Manuscript Author Manuscript Author Manuscript

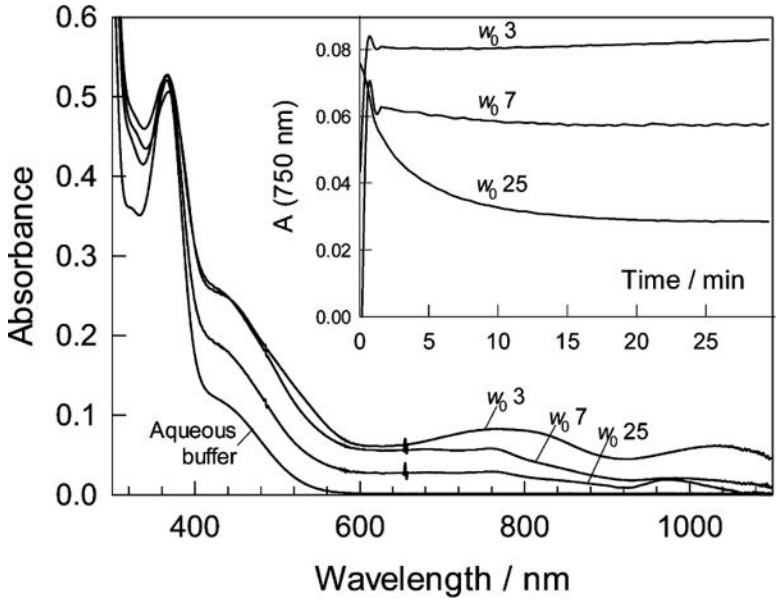

Figure 2.

Spectra of **1a** in the AOT reverse micelles in *n*-octane recorded 20 min after mixing all components. The spectrum of **1a** in the aqueous buffer (bottom) is shown for comparison. Conditions: [**1a**] 1.36×10^{-4} M, pH 8, w_0 = 3, 7, and 25; 25 °C. Inset shows changes of absorbance at 750 nm with time for the three different values of w_0.

Author Manuscript Author Manuscript Author Manuscript Author Manuscript

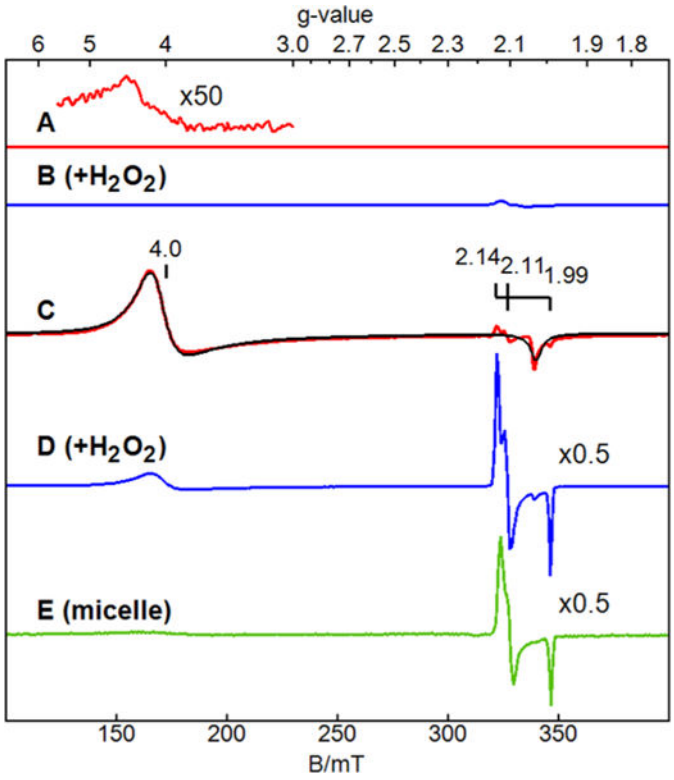

Figure 3.

EPR spectra (ν = 9.651 GHz, T = 15 K) of **1a** at pH 12 under different conditions. A: **1a**; B: **1a** + 1 equiv of H_2O_2; C: **1a** in 50% glycerol; D: **1a** + 1 equiv of H_2O_2 in 50% glycerol; E: **1a** in reverse micelles (w_0 10, pH 12). The spectral intensities are displayed for equal concentrations of **1a**, with additional scale factors as displayed. The black line on C is a simulation for S = 3/2, D = +2.5 cm^{-1}, E/D = 0, g = 2.045, 2.05, 2.03, σ_g = 0.15, 0.15, 0.02). The species percentages are stated in the text. A small variable amount (~2%) of **3a** is generated in air without H_2O_2, which is presumed to be reaction of **1a** with low levels of dioxygen.

Author Manuscript Author Manuscript Author Manuscript Author Manuscript

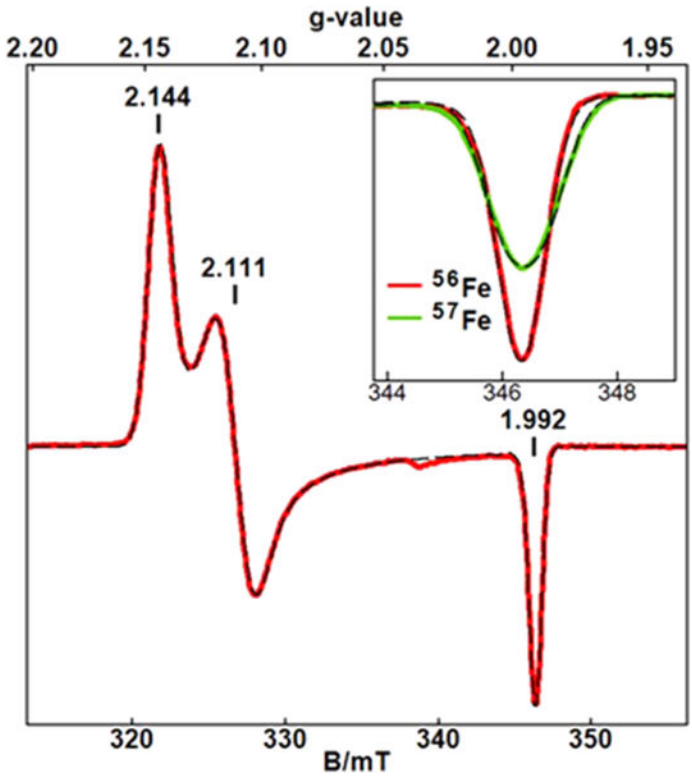

Figure 4.

EPR spectra (red and green) of **3a** under the same conditions as in Figure 3D. The inset shows an expanded view at $g = 1.992$ for ^{56}Fe and enriched ^{57}Fe samples. The dashed lines are $S = 1/2$ simulations with and without inclusion of a hyperfine term for $I = 1/2$ with $A =$ 18 MHz.

Author Manuscript Author Manuscript Author Manuscript Author Manuscript

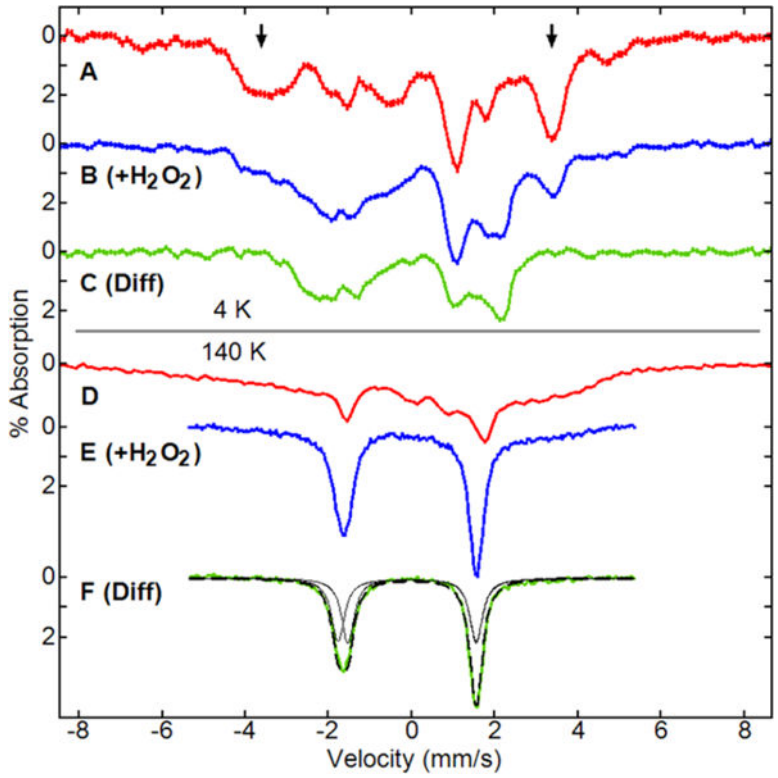

Figure 5.

Mössbauer spectra with a parallel field of 45 mT at 4.2 K (A–C) and 140 K (D–F) of (A, D) **1a** at pH 11.8 (0.1 M phosphate), 50% glycerol; (B, E) **1a** + 1 equiv of H_2O_2, added at −20 °C; and (C, F) **3a**, $Fe^{III}Fe^{IV}$. The spectra of $Fe^{III}Fe^{IV}$ are subtractions of 45% of the spectra of **1a** from the spectra with **1a** + H_2O_2. At 140 K (F), the simulation (dashed line) is for two quadrupole doublets with equal area (solid black lines) with parameters given in the text.

Author Manuscript Author Manuscript Author Manuscript Author Manuscript

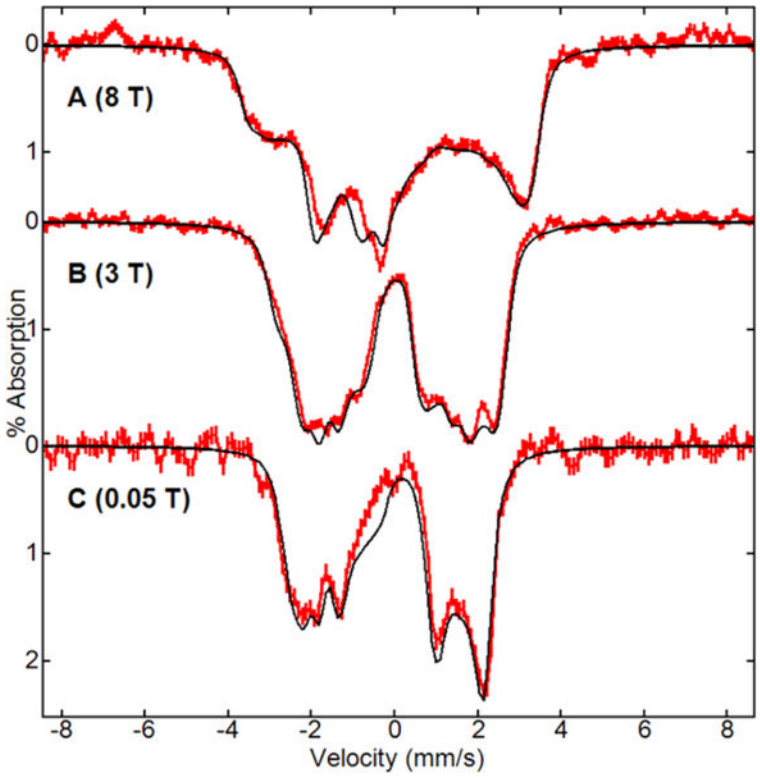

Figure 6.

Mössbauer spectra (red lines) of **3a** at pH 11.8, 50% glycerol, 1 equiv of H_2O_2 recorded at 4.2 K with an applied field of 8 T (A), 3 T (B), and 0.05 T (C). The spectra are after subtraction of 45% of the area the corresponding spectra of **1a**. Simulations (black lines) are for Fe^{III} and Fe^{IV} sites: $J = -30$ cm^{-1}, $S_3 = 1.5$, $D_3 = 3.2$ cm^{-1}, $E/D_3 = 0.18$, $\mathbf{A}_3 = (-45, -120, 55)$ MHz, $S_4 = 1$, $D_4 = 21$ cm^{-1}, $E/D_4 = 0.13$, $\mathbf{A}_4 = (-112, -151, 110)$ MHz for the values of δ and ΔE_Q given in the text.

Author Manuscript Author Manuscript Author Manuscript Author Manuscript

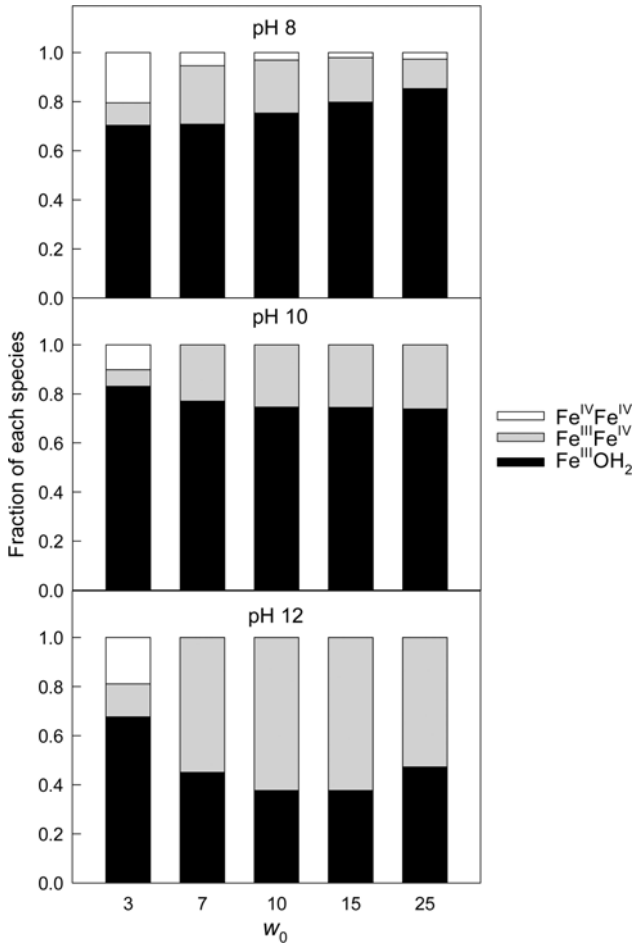

Figure 7.

Estimated fractions of $Fe^{III}OH_2$, $Fe^{III}Fe^{IV}$, and $Fe^{IV}Fe^{IV}$ (all derived from **1a**) in the AOT reverse micelles at different pH and w_0. For other conditions, see caption to Figures 2 and S1 (SI).

Author Manuscript Author Manuscript Author Manuscript Author Manuscript

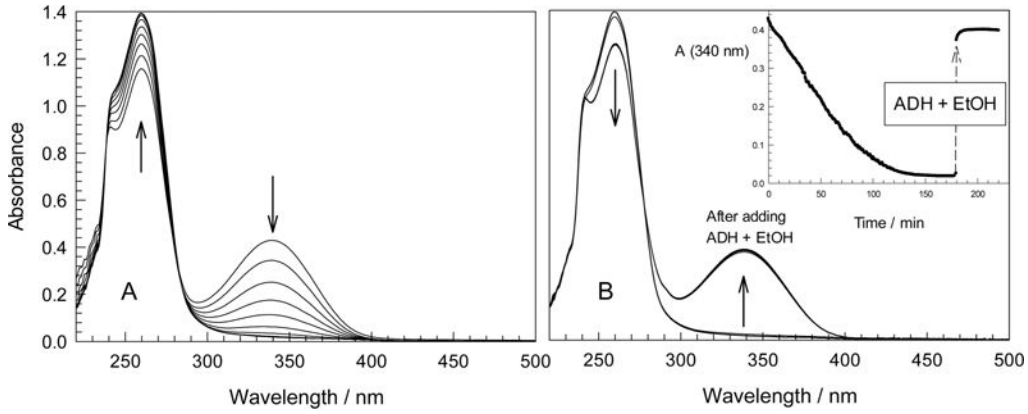

Figure 8.

(A) Spectral changes that accompany **1a**-catalyzed oxidation of NADH into NAD^+ by O_2 and (B) regeneration of NADH by ADH/EtOH. Time interval between spectra shown in A is 20 min (scans were made every 30 s). ADH (from *Saccharomyces cerevisiae*, 0.7 mg, 210 units in 50 μL water) and 10 μL of EtOH were added to the reaction mixture after 3 h followed by vigorous shaking. Inset in B illustrates the time scale of TAML-catalyzed oxidation and the enzyme-catalyzed regeneration of NADH. Conditions: 0.1 M AOT, 0.01 M carbonate (pH 10), w_0 7; [**1a**] 2.46×10^{-6} M, [NADH] 9.9×10^{-5} M.

Author Manuscript Author Manuscript Author Manuscript Author Manuscript

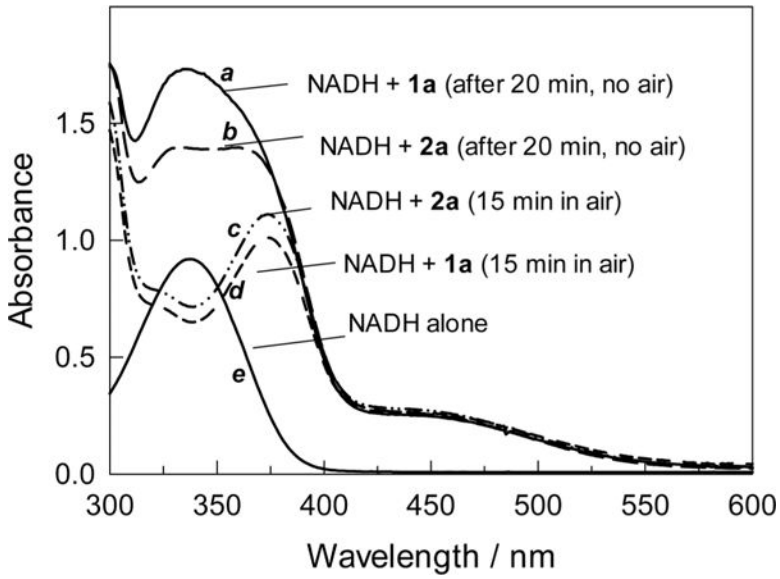

Figure 9.

UV–vis spectra of NADH in the presence of **1a** or **2a** (1.5 mL methanol was added to 1.5 mL reaction mixture to quench the reaction). Conditions: w_0 7, pH 12, [NADH] 2.1×10^{-4} M, [total iron] = 2.0×10^{-4} M. (a, b: spectra of NADH reacted with **1a** or **2a** in the absence of O_2; c, d: spectra of NADH reacted with **1a** or **2a** after exposure to air for 15 min; e: spectrum of NADH alone).

Author Manuscript Author Manuscript Author Manuscript Author Manuscript

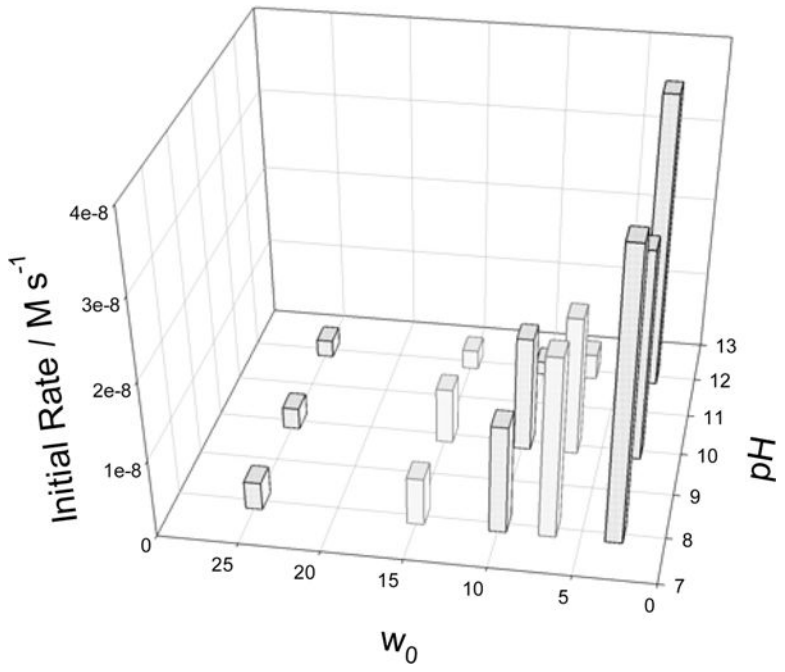

Figure 10.

Initial rates of NADH oxidation catalyzed by **1a** in reverse micelles. Conditions: [**1a**] 2.5×10^{-6} M, [NADH] 5.1×10^{-5} M, the flash frequency is 30 s. See text for explanations.

Author Manuscript Author Manuscript Author Manuscript Author Manuscript

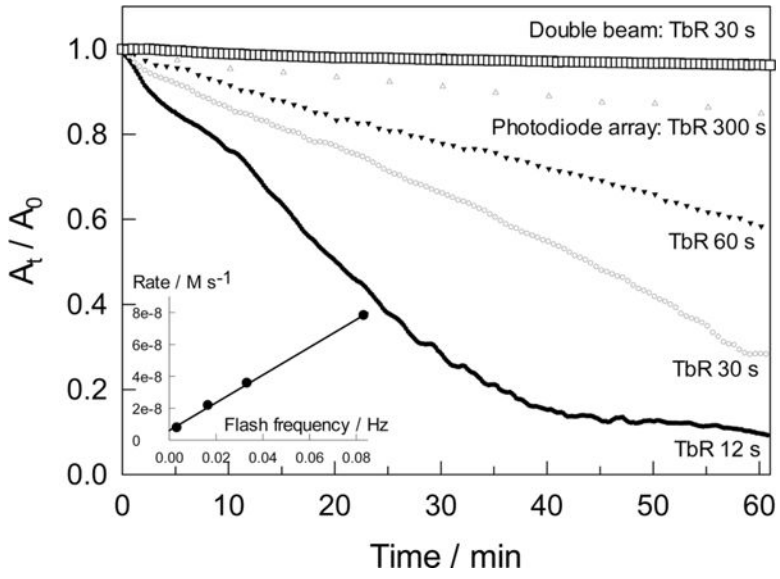

Figure 11.

Kinetics of NADH oxidation registered by different UV–vis spectrometers applying different pulse frequencies. The top curve was obtained using a double beam instrument, and lower curves were produced using a photodiode array instrument. TbR is the time between recordings of successive spectra. Other conditions: pH 10, w_0 10, [NADH] 5.14×10^{-5} M, [**1a**] 2.39×10^{-6} M.

Author Manuscript Author Manuscript Author Manuscript Author Manuscript

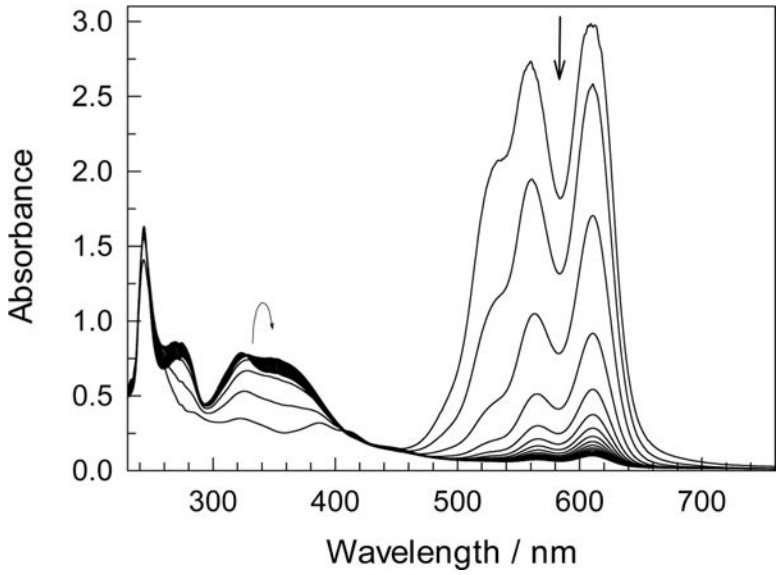

Figure 12.

Spectral changes that accompany **1a**-catalyzed oxidation of PNC by O_2 in the reverse micelles. Conditions: [PNC] 4.5×10^{-5} M, [**1a**] 5.0×10^{-6} M, w_0 10, pH 10, spectra shown with 10 min intervals.

Author Manuscript Author Manuscript Author Manuscript Author Manuscript

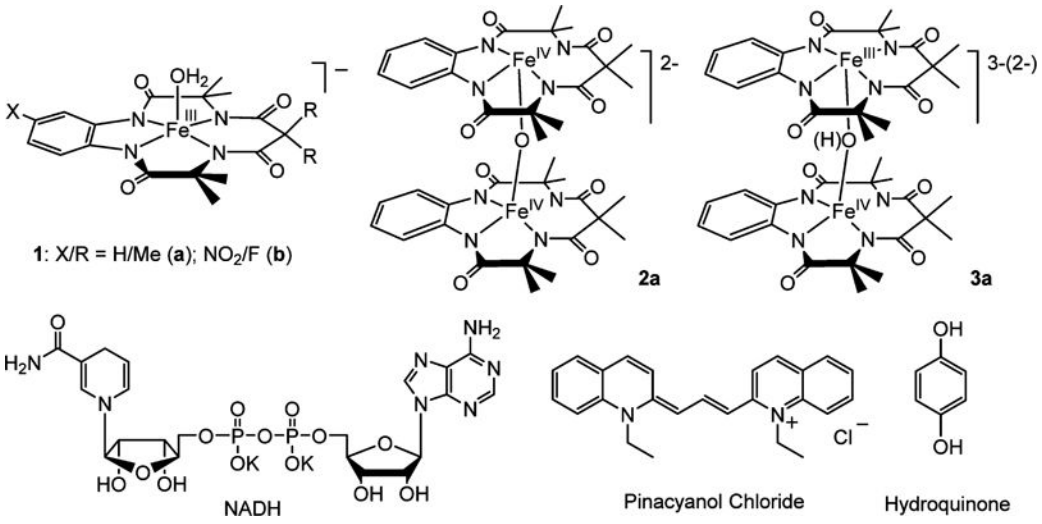

Chart 1.

Compounds Used in This Study Including the Catalysts 1a and 1b, the Known Homovalent μ-Oxo-Bridged Iron(IV) Dimer 2a and Heterovalent μ-Oxo(hydroxo)-Bridged Iron(IV/III) Dimer 3a Characterized in This Work, and the Substrates β-Nicotinamide Adenine Dinucleotide, Reduced Dipotassium Salt (NADH), Pinacyanol Chloride (PNC), and Hydroquinone (HQ)

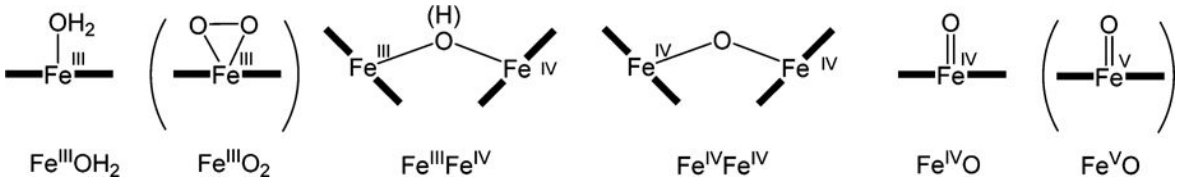

Chart 2. Iron Species That Could Coexist in the Reverse Micelles[a]

[a] $Fe^{III}Fe^{IV}$ was unknown prior to this work. Species in parentheses were obtained in MeCN.

Author Manuscript Author Manuscript Author Manuscript Author Manuscript